Neuroscience 300 (2015) 325–337

DESCENDING AND TONOTOPIC PROJECTION PATTERNS FROM THE AUDITORY CORTEX TO THE INFERIOR COLLICULUS

M. M. STRAKA, [a]* **R. HUGHES,** [a] **P. LEE** [a] **AND H. H. LIM** [a,b,c]

[a] *Department of Biomedical Engineering, University of Minnesota, Twin Cities, 312 Church St SE, Minneapolis, MN 55455, United States*

[b] *Institute for Translational Neuroscience, University of Minnesota, Twin Cities, Minneapolis, MN 55455, United States*

[c] *Department of Otolaryngology, Head and Neck Surgery, University of Minnesota, Twin Cities, 516 Delaware Street SE, Minneapolis, MN 55455, United States*

Abstract—The inferior colliculus (IC) receives many corticofugal projections, which can mediate plastic changes such as shifts in frequency tuning or excitability of IC neurons. While the densest projections are found in the IC's external cortices, fibers originating from the primary auditory cortex (AI) have been observed throughout the IC's central nucleus (ICC), and these projections have shown to be organized tonotopically. Some studies have also found projections from other core and non-core cortical regions, though the organization and function of these projections are less known. In guinea pig, there exists a non-core ventrorostral belt (VRB) region that has primary-like properties and has often been mistaken for AI, with the clearest differentiating characteristic being VRB's longer response latencies. To better understand the auditory corticofugal descending system beyond AI, we investigated if there are projections from VRB to the ICC and if they exhibit a different projection pattern than those from AI. In this study, we performed experiments in ketamine-anesthetized guinea pigs, in which we positioned 32-site electrode arrays within AI, VRB, and ICC. We identified the monosynaptic connections between AI-to-ICC and VRB-to-ICC using an antidromic stimulation method, and we analyzed their locations across the midbrain using three-dimensional histological techniques. Compared to the corticocollicular projections to the ICC from AI, there were fewer projections to the ICC from VRB, and these projections had a weaker tonotopic organization. The majority of VRB projections were observed in the caudal–medial versus the rostral–lateral region along an isofrequency lamina of the ICC, which is in contrast to the AI projections that were scattered throughout an ICC lamina. These findings suggest that the VRB directly modulates sound information within the ascending lemniscal pathway with a different or complementary role compared to the modulatory effects of AI, which may have implications for treating hearing disorders.

Key words: corticofugal, feedback, auditory cortex, inferior colliculus, tonotopy, modulation.

INTRODUCTION

Traditionally, anatomical tracer studies have found that corticocollicular fibers from core and belt cortices primarily terminate in the nonlemniscal external cortices of the IC rather than the lemniscal ICC (Faye-Lund, 1985; Huffman and Henson, 1990; Herbert et al., 1991; Winer et al., 1998). However, there has been growing anatomical evidence that ICC receives direct, tonotopically-organized projections from core auditory areas including the primary auditory cortex, AI (Andersen et al., 1980; Feliciano and Potashner, 1995; Saldana et al., 1996; Budinger et al., 2000; Bajo and Moore, 2005; Coomes et al., 2005; Bajo et al., 2007; Lim and Anderson, 2007a; Malmierca and Ryugo, 2011). Studies in rat (Saldana et al., 1996), cat (Andersen et al., 1980), and ferret (Bajo et al., 2007) show that these projections are bilateral, though studies in gerbil (Budinger et al., 2000; Bajo and Moore, 2005) and in guinea pig (Coomes et al., 2005) found that the majority of these projections are ipsilateral. These corticofugal projections may influence plastic changes within the ICC, since there have been numerous studies showing that frequency tuning of ICC neurons can be finely shifted toward those of electrically stimulated AI neurons (Yan and Suga, 1998; Yan et al., 2005; Xiong et al., 2009). A more recent study also showed that electrical stimulation of AI neurons could cause extensive suppression of excitability of neurons in the ICC when paired with broadband noise stimulation (Markovitz et al., 2013). Less is known about corticofugal fibers that originate from non-AI cortical regions and target the ICC. In general, most studies have shown that only primary or core cortical regions project to the ICC (Winer et al., 1998; Bajo and Moore, 2005; Winer, 2005; Bajo et al., 2007), though one study found that the ICC also receives projections from non-core fields (Budinger et al., 2000). It is unknown whether these corticofugal projections from non-core regions are also tonotopically or topographically organized to the ICC and if

*Corresponding author. Address: 3400 N. Charles St, Ames 22, Psychological and Brain Sciences Department, Johns Hopkins University, Baltimore, MD 21218, United States.
E-mail address: margo.straka@jhu.edu (M. M. Straka).

Abbreviations: ΔBF, difference in the best frequencies between two sites; AC, auditory cortex; AI, primary auditory cortex; BF, best frequency; CSD, current source density; CYO, cytochrome oxidase; DC, dorsocaudal area; FRM, frequency response map; FSL, first-spike latency; IC, inferior colliculus; ICC, central nucleus of the inferior colliculus; PSTH, post-stimulus time histogram; VAF, ventral auditory field; VRB, ventrorostral belt.

http://dx.doi.org/10.1016/j.neuroscience.2015.05.032
0306-4522/

they serve a different descending functional role compared to A1. Understanding the varying roles of the descending pathways from different cortical regions will improve our understanding of how the brain modulates ascending coding of auditory information for perception and learning. Clinically, it could also open up new targets and improve neural stimulation devices for treating hearing disorders, considering that patients are currently being implanted with electrode arrays that stimulate non-core or secondary auditory cortical regions for treating tinnitus (Friedland et al., 2007; De Ridder et al., 2011; Vanneste and De Ridder, 2012; Zhang, 2013; Engelhardt et al., 2014) but with very little understanding of the modulatory effects on the auditory system.

In the guinea pig, there is a non-core area called the ventrorostral belt, (VRB) (Wallace et al., 2000) that exhibits primary-like coding properties and was not differentiated from AI in early studies (Redies et al., 1989a,b). Located ventral and lateral to AI, neurons in VRB respond to frequency tones with low thresholds and are organized in a tonotopic pattern parallel to that of AI, thus causing the tonotopy to appear as a continuum of AI (Wallace et al., 2000). Originally distinguished from AI because of its long latencies and poor responses to noise (Wallace et al., 1999), VRB has also been shown to have the most units of all cortical fields that can discriminate conspecific vocalizations using a rate code (Grimsley et al., 2012). In terms of histological labeling, there are no clear transitions between AI and VRB for either myelin or cytochrome oxidase (**CYO**) staining (Wallace et al., 2000). VRB has moderate staining of myelin, less than the dense labeling in AI but similar to another core region called the dorsocaudal area (**DC**) (Wallace et al., 2000). In addition, VRB has dense labeling of CYO similar to that of AI and greater than the moderate labeling in DC. A previous study found that VRB does project to the inferior colliculus (IC) (Schofield, 2009), but it is unknown whether the VRB has direct projections to the ICC, or how they compare to those from AI.

In this study, we investigated the monosynaptic projection pattern from VRB to ICC and compared it to the pattern from AI to ICC within the anesthetized guinea pig. Because the small size of the VRB limits the ability to use tracer techniques for characterizing the precise spatial and functional organization of its corticofugal projections to the ICC, we used a previously developed antidromic stimulation technique (Lim and Anderson, 2007a), which allowed us to map descending projections between and characterize the physiological features of cortical and collicular neurons in the same animal. We found that both AI and VRB project to the ICC in a tonotopic manner, though with distinct differences in their projection pattern across and along the ICC laminae. These results suggest that AI and VRB have varying roles in processing both ascending and descending sound information within the lemniscal pathway.

EXPERIMENTAL PROCEDURES

Overview

Basic surgical procedures and methods for neural recording and stimulation were similar to those presented in previous work (Lim and Anderson, 2006, 2007a; Straka et al., 2013). Ketamine-anesthetized guinea pigs were used in accordance with policies of the University of Minnesota's Institutional Animal Care and Use Committee. Silicon-substrate, 32-site Michigan electrode arrays (NeuroNexus Technologies, Ann Arbor, MI, USA) were used to electrically stimulate the ICC and record the corresponding neural responses within the auditory cortex (**AC**). Appropriate placement of the array sites within the ICC and AC was guided by acoustic-driven responses (Wallace et al., 2000; Snyder et al., 2004; Lim and Anderson, 2007b). Array sites in the ICC were individually stimulated and multi-unit spiking responses were recorded in AI and VRB. When antidromic activity was detected in AI or VRB, the minimal stimulation threshold and location across the ICC was found and analyzed to determine if there is a spatial distribution across the ICC lamina for corticofugal projections.

Surgery

Experiments were performed on 23 Hartley guinea pigs (380 ± 53 g, Elm Hill Breeding Labs, Chelmsford, MA, USA). Animals were initially anesthetized with an intramuscular injection of ketamine (40 mg/kg) and xylazine (10 mg/kg), and were given periodic supplements to maintain an areflexic state. After fixing the animal into a stereotaxic frame (David Kopf Instruments, Tujunga, CA, USA), the right side of the cortex was exposed from the caudal end of the occipital lobe to the middle cerebral artery of the temporal lobe. The dura was removed, micromanipulators were used to insert the arrays into the ICC and AC, and the exposed brain was covered with agarose gel.

Stimulation and recording setup

All experiments were performed in an acoustically- and electrically-shielded chamber and controlled by a computer interfaced with TDT System 3 hardware (Tucker-Davis Technology, Alachua, FL, USA) using custom software written in MATLAB (MathWorks, Natick, MA, USA). For acoustic stimulation, sound was presented via a speaker coupled to the left ear through a hollow ear bar. The speaker-ear bar system was calibrated using a 0.25-in. condenser microphone (ACO Pacific, Belmont, CA, USA) connected to the ear bar via a short plastic tube representing the ear canal.

All neural signals were passed through analog DC-blocking and anti-aliasing filters from 1.6 Hz to 7.5 kHz. The sampling frequency used for acoustic stimulation was 195 kHz and for neural recording was 24 kHz. Electrical stimulation up to 64 μA was presented on different sites on the ICC array in a monopolar configuration with a ground return in the neck muscles. The pulses were biphasic, charge-balanced, cathodic-leading, and 205-μs/phase. The recording ground needle was positioned either under the skin approximately 2 cm rostral to bregma or directly in the brain in the parietal lobe. No obvious differences in results were observed when using the different recording grounds.

Placement of arrays

Post-stimulus time histograms (**PSTHs**) and frequency response maps (**FRMs**) of spiking activity were plotted online to confirm the array's position within the AC and the ICC. Details on these analysis methods and example plots for similar types of arrays are presented in previous publications (Lenarz et al., 2006; Lim and Anderson, 2006; Neuheiser et al., 2010; Straka et al., 2013). Briefly, the electrical artifact was removed by inserting null values for 1.5 ms after stimulus onset, the neural signals were bandpass filtered (300–3000 Hz), and spikes were detected when the signal exceeded a threshold of three standard deviations above the background activity. For FRMs, four trials were presented for each pure tone (1–40 kHz, eight steps/octave) and level (0–70 dB, 10-dB steps) stimulus. The best frequency (**BF**) was taken as the centroid of frequencies that elicited spiking responses at 10 dB above the visually-determined threshold.

The AC array consisted of four 5-mm-long shanks separated by 400 μm. Sites were linearly spaced at 200 μm along the shank and each had an area of 177 μm^2. The array was inserted approximately perpendicular to the cortical surface in an attempt to align each shank along a cortical column in AC (Abeles and Goldstein, 1970; Redies et al., 1989b; Wallace et al., 2000). Placement into AI or VRB was confirmed when tonotopic shifts from low to high BFs were observed from ventral-and-rostral to dorsal-and-caudal locations (Wallace et al., 2000). To investigate differences across AC locations, we reconstructed the site locations on the cortical surface based on microscope images (OPMI 1 FR pro, Zeiss, Dublin, CA, USA) taken of our array placements and normalized based on various landmarks (e.g., middle cerebral artery, bregma and lateral suture lines, major blood vessels) as successfully used in previous studies (Schreiner et al., 2000; Wallace et al., 2000; Eggermont and Roberts, 2004). These normalized locations and their respective BFs can be seen overlaid on the AC in Fig. 1.

Data were analyzed on a total of 88 AI placements from 20 guinea pigs and 20 VRB placements from four guinea pigs, where multiple AC placements were made in two guinea pigs. AC placements were determined to be in AI or VRB by the location on the cortex seen in Fig. 1, where VRB placements were more lateral and ventral than AI placements. These locations are similar to those previously determined in guinea pig (Wallace et al., 2000; Grimsley et al., 2012). The identification of locations was confirmed by differences in the first-spike latency (**FSL**) responses, which are significantly longer in VRB (Wallace et al., 2000). The FSL was calculated by computing the mean latency of the first spike to noise stimuli at 70-dB SPL across 100 trials, and the FSL for a specific cortical shank was determined by averaging across all sites that responded to noise. Across all the AC locations, the mean FSL for AI was 21 ± 5 ms (N = 85 sites), which was significantly different from the mean VRB FSL of 33 ± 5 ms (N = 18 sites), ($P < 3 \times 10^{-10}$ using two-tailed, unequal variance t-tests, sites that responded weakly to noise were not included). Thus, we were confident that VRB and AI were appropriately differentiated. Given the relatively fewer number of VRB sites, the results may not represent all VRB neurons or completely map out the entire VRB. However, given the relatively small size of VRB (see Fig. 1), which extends about 2.5 mm rostral to caudal and 1 mm medial to lateral, and the size of our electrode array (1.2 mm between the first and fourth shank) each placement spanned approximately half of the VRB. In addition, we performed one experiment with two VRB placements, as well as an AI placement, that had consistent results as our pooled data across animals. Therefore, we believe the results we found between AI and VRB are representative of the two fields.

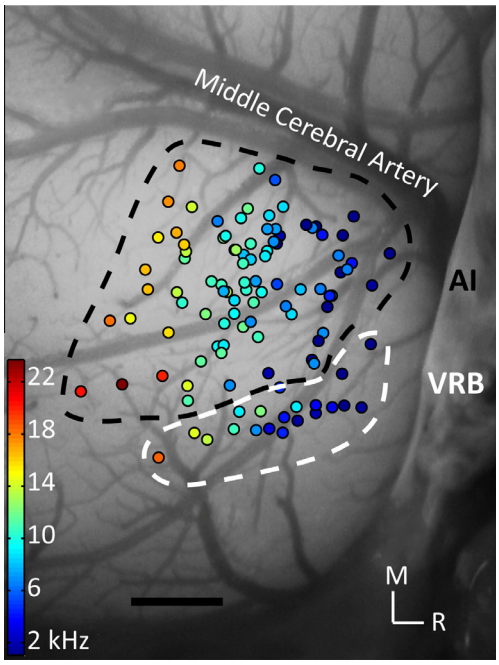

Fig. 1. The location and BF of each recording site in the auditory cortex, overlaid on a typical guinea pig cortex. Sites were determined to be in AI or VRB based on cortical location as well as FSL responses (see *Experimental procedures: Placement of arrays*). Black scale bar = 1 mm. R, rostral; M, medial.

As seen in Fig. 2A, the identification of AC layers was accomplished by performing current source density (**CSD**) analysis (Muller-Preuss and Mitzdorf, 1984; Mitzdorf, 1985; Kral et al., 2000) in response to 70-dB SPL broadband noise (100 trials) using the finite difference formula:

$$\mathrm{CSD}(z) = \sigma_z \frac{\phi(z+\Delta z) - 2\phi(z) + \phi(z-\Delta z)}{(\Delta z)^2}$$

where ϕ is the averaged LFP across trials, z is the depth location of each site along an AC array shank, Δz is the differentiation step size, and σ_z is the component of conductivity in the z-direction. Δz was equal to the AC site spacing of 200 μm and σ_z was set to one since absolute CSD values were not required for analysis. The one-dimensional CSD approximation provides a consistent representation for the current sinks and sources associated with columnar synaptic activity in the guinea pig AC (Lim and Anderson, 2007a; Middlebrooks, 2008). The main input layer of AC, which is layer III/IV in

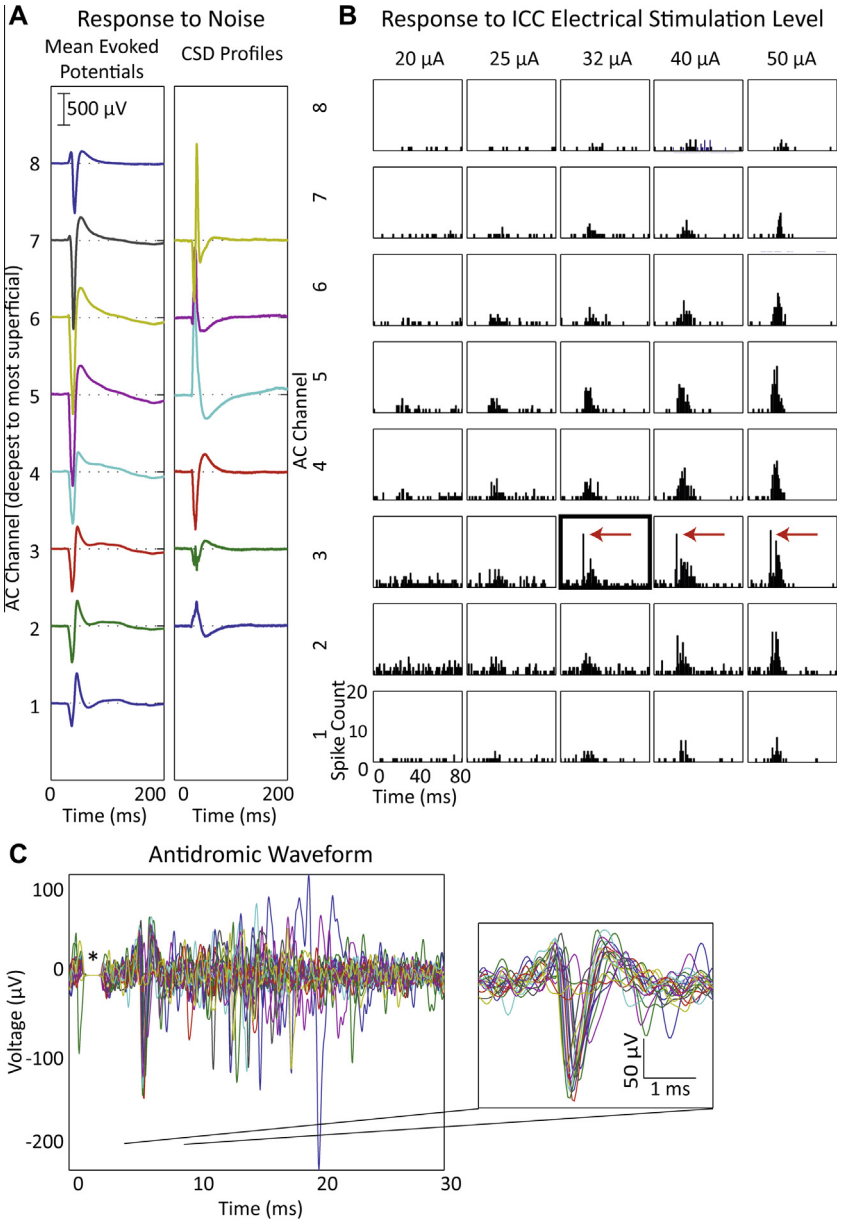

Fig. 2. An example identifying antidromic activation of an AC site along a cortical column. Responses to 70-dB SPL broadband noise were recorded for all eight sites along a shank that was placed along a cortical column. Local field potential responses were averaged across 20 trials to find the mean evoked potential (A). CSD analysis was performed across all of the sites (except channel 1 and 8, given that CSD analysis requires responses in neighboring sites for the spatial derivative calculation). Channel 3 was identified as being in layer V, since it was two sites below channel 5, the shortest latency current sink corresponding to the main input layers III/IV (see *Experimental procedures: Placement of arrays* for more information on CSD analysis). Spiking activity in response to electrical stimulation of the ICC were recorded and summarized with PSTHs of activity (B). A stimulation level of 25 µA did not evoke obvious antidromic activity on site 3 that could be considered above baseline. However, a suddenly strong and temporally precise antidromic response (red arrow) could be observed on site 3 (i.e., layer V; thick outlined black box) with just a slight increase of current level of 2 dB (i.e., at 32 µA for threshold) and for higher levels. Neural data of all 20 trials recorded on channel 3 at threshold is plotted (**C**), with the inlay showing temporally precise spiking indicative of antidromic activity. Note that the electrical artifact, denoted by the asterisk, was removed. (For interpretation of the references to colour in this figure legend, the reader is referred to the web version of this article.)

guinea pig (Huang and Winer, 2000; Smith and Populin, 2001), corresponded to the site with the shortest latency current sink (i.e., positive CSD peak). The main output layer V was identified as being two or three electrode sites (~400–600 µm) deeper than the layer III/IV site (Wallace et al., 2000; Lim and Anderson, 2007a), typically having a current source (i.e., negative CSD peak). For the example in Fig. 2A, these criteria were used to determine that channel 5 is in layer III/IV and channel 3 is in layer V.

Since CSD analysis has not been well described in VRB, we further verified the recording of layer V neurons by comparing the cortical depth from sites in layer II to layer V to anatomical measurements. For each shank, we first found the shallowest site along each shank with spiking responses to 100 trials of broadband noise at 70-dB SPL. Given that layer I has few neurons while layer II has ample pyramidal neurons (Schofield and Coomes, 2006; Wallace and Palmer,

2008), this shallow site was referred to as the layer II site. On average, sites identified as layer V were 920 ± 160 μm below layer II for AI (N = 87 layer differences) and 860 ± 170 μm below layer II for VRB (N = 18). Note that our resolution was limited to the 200-μm sites spacing, and placements where shallow sites were broken or did not respond to noise were not included. Anatomical analysis using multiple staining preparations in guinea pig found that the ventral (i.e., deeper) border of layer V is approximately 1190 μm below the ventral border of layer II for AI, though this value could vary between 580 and 1470 μm when comparing the distance between the closest and farthest borders of the cortical layers (Wallace and Palmer, 2008). Though it is unclear what depths correspond to specific layers in the VRB, cortical thickness has typically been found to be thinner in belt regions, though thickness could vary from 1.6 to 2.2 mm in comparison to the typical thickness of 2 mm in AI (Grimsley et al., 2012). The consistent range of values in our study with these expected anatomical depths supports that the CSD analysis is correctly identifying sites in layer V.

The ICC array consisted either of four 8-mm-long shanks or of two 10-mm-long shanks. For both arrays, each shank was separated by 500 μm and sites were linearly spaced at 100 μm along the shank. Each site had an area of approximately 700 μm^2. Prior to the experiment, the sites on the ICC array were activated using cyclic voltammetry to enable both recording and stimulation up to 100 μA (Anderson et al., 1989; Lim and Anderson, 2006). The ICC array was placed at a 45° angle to the sagittal plane through the visual cortex in order to be aligned along the tonotopic axis of the ICC (Malmierca et al., 1995; Snyder et al., 2004). Proper array placement in the ICC was confirmed by observing FRMs that exhibited an orderly shift from low to high BFs from superficial to deeper locations along a shank (Snyder et al., 2004; Lim and Anderson, 2006).

Electrical stimulation and data analysis

For each ICC array placement, electrical stimulation was presented individually on several sites at stimulation levels from 16 to 36 dB in 2-dB steps (i.e., 6.3–64 μA), while randomizing level and stimulation site. We did not stimulate at higher levels in order to remain within the threshold limits for safety and stability of our electrode arrays. Stimulation evoked multi-unit spiking activity in the AC, with antidromic activity often present in layer V. As characterized in a previous publication (Lim and Anderson, 2007a), antidromic activity was determined when the spikes exhibited short latencies with low temporal jitter (< 1 ms), the activity was predominantly isolated in layer V, and a slight increase in current level above the threshold resulted in a sudden increase from no activity to robust spiking per trial. Though more definitive tests for antidromicity include spike collisions and high stimulation following rates (Lipski, 1981; Mitani and Shimokouchi, 1985; Rose and Metherate, 2001), Lim and Anderson (2007a) observed that these characteristics listed above sufficiently identified the AI-to-ICC projections.

We used these characteristics to determine antidromic activity in layer V, as shown in Fig. 2B, C. Fig. 2B, C shows an example of short-latency, temporally precise spiking in layer V (channel 3 based on CSD in Fig. 2A) that had suddenly exceeded threshold to robust spiking (for nearly all 20 trials) with just a slight increase in current (i.e., our smallest step of 2 dB). It can be seen in Fig. 2C that the spike waveform is similar in shape and timing across almost all 20 trials. A few trials had a distorted or nonexistent spike, which is possible due to external noise or if a spike normally happened along that neuron's axon at the same time we electrically activated it antidromically to block the spike propagation to AI (i.e., spike collision). Note that the short latency, temporally precise spiking characterizing the antidromic activity contrasts to the longer latency, temporally broad spiking characterizing the orthodromic activity, as seen in Fig. 2B (also see Fig 3A). For comparison, we found the FSLs for the antidromic activity and for the orthodromic responses at threshold (i.e., when spiking was visually determined to be stronger than background activity) in layer V sites. Histograms for all FSLs for antidromic and orthodromic evoked activity are shown in Fig. 3B. The mean FSL for antidromic activity was 7.2 ± 3.0 ms (N = 288 AC–IC pairs), which was significantly shorter than the mean FSL for orthodromic activity of 15.7 ± 3.7 ms (N = 542 AC–IC pairs) ($P < 1.8 \times 10^{-103}$ using the Mann–Whitney U test). For each stimulation-recording ICC–AC site pairs with antidromic activity, we obtained the stimulation threshold for further analysis. Out of all 288 AC–IC pairs, we observed only three cases with two distinct antidromic peaks in the PSTH, and all of these were in A1. In these cases, we analyzed the response with the lowest threshold.

This method for identifying antidromic activity also allowed us to detect some unusually long-latency antidromic spikes. For example, the longest FSL for antidromic activity was 24.2 ms (in Fig. 3B). Despite its long latency, this activity had several features indicative of antidromic activity, including occurring at a site in layer V (channel 2 in Fig. 3C, D), having a drastic increase of activity at threshold from no activity to robust spiking with only a 2-dB increase in current (Fig. 3D), and being extremely precise temporally (Fig. 3D, E). In addition, this antidromic activity occurred when there was no orthodromic activity at any other site, even at our highest current levels. While most antidromic latencies are below 10 ms (Mitani and Shimokouchi, 1985; Schofield et al., 1987; Lim and Anderson, 2007a), some very thin, slow conducting axons have been shown to have latencies exceeding 40 ms (Ferster and Lindstrom, 1983; Swadlow, 1998). Given that the example in Fig. 3C–E followed our specific characteristics for antidromic activity, it appears likely that this monosynaptic projection may be a thin, slow conducting axon.

Histological reconstructions

Prior to placement, the ICC array was dipped in a red stain (Di-I: 1,1-dioctadecyl-3,3,3′,3′-tetramethylindocarbocyanine perchlorate, Sigma–Aldrich, St. Louis, MO,

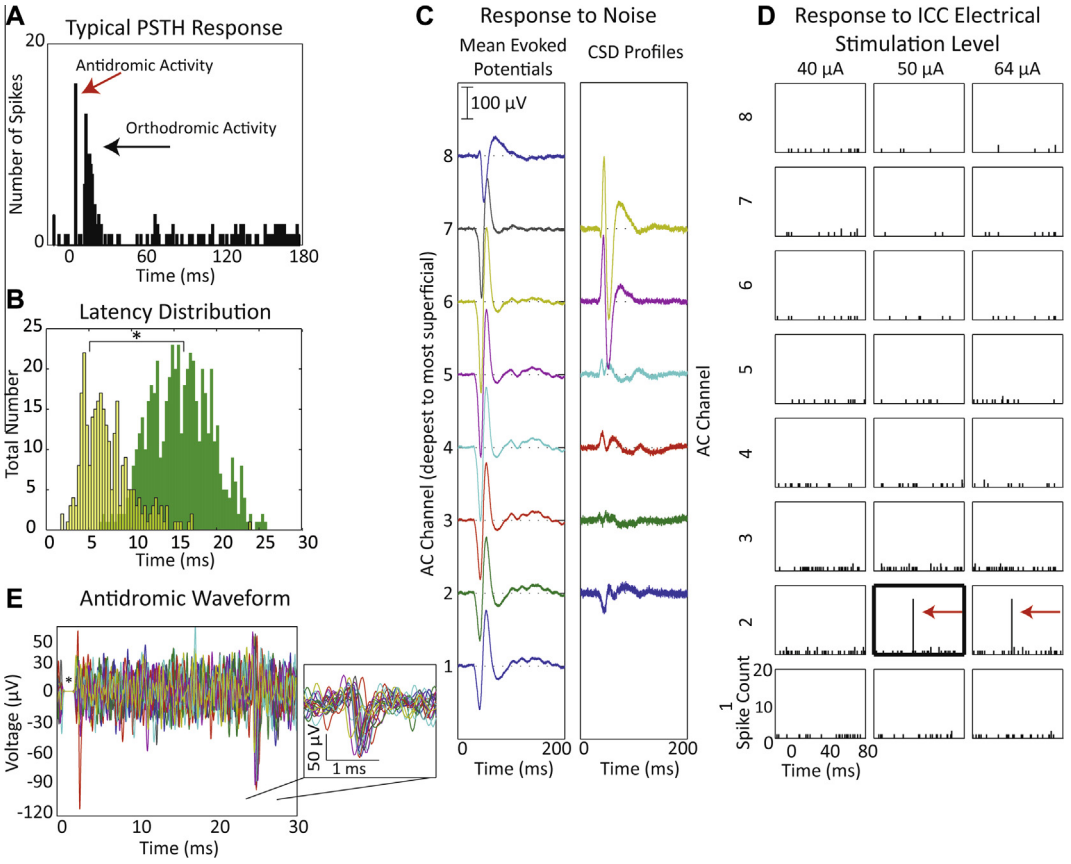

Fig. 3. (A) A typical PSTH response contrasting evoked antidromic activity and orthodromic activity on a site in layer V. While antidromic activity is typically characterized by a short latency, temporally precise response, orthodromic activity has a longer latency and temporally broad response. (B) The FSL of antidromic activity at threshold was found and compared to orthodromic activity at threshold. Antidromic activity was significantly shorter than orthodromic activity ($P < 1.8\times10^{-103}$, see *Experimental procedures: Electrical stimulation and data analysis*). (C–E) Data for the antidromic activity with the longest latency case observed in B. Local field potential responses to 70-dB SPL broadband noise were recorded across sites placed along a cortical column and averaged across 20 trials (C). CSD analysis was performed and used to identify the shortest latency current sink corresponding to the main input layers III/IV to be between channels 4 and 5, and channel 2 as layer V, being two sites below channel 4 and having a current source (see *Experimental procedures: Placement of arrays* for more information on CSD analysis). Spiking activity in response to electrical stimulation of the ICC was recorded and summarized with PSTHs of activity (B). A stimulation level of 40 µA did not evoke activity, but sudden, strong, temporally precise antidromic activity (red arrow) can be observed in channel 2 (i.e., layer V; thick outlined black box) at 50 µA, the threshold, and at 60 µA. Neural data of all 20 trials recorded on channel 2 at threshold is plotted (C), with the inlay showing temporally precise spiking indicative of antidromic activity. Note that the electrical artifact, denoted by the asterisk, was removed. (For interpretation of the references to colour in this figure legend, the reader is referred to the web version of this article.)

USA) to later identify an array position within the ICC during histological analysis. Detailed description of the histological procedure, midbrain reconstruction, normalization, and approximation of frequency laminae is provided in a previous publication (Markovitz et al., 2012). Briefly, the midbrain was fixed with 3.7% paraformaldehyde and cryosliced into sagittal sections of 60-µm widths using a sliding microtome (Leica, Buffalo Grove, IL, USA). Images of each slice were taken using a Leica MZ FLIII fluorescence stereomicroscope (Leica, Buffalo Grove, IL), Leica DFC412 C peltier cooled CCD camera, and Image-Pro software (MediaCybernetics, Bethesda, MD, USA). A single reflection white light image using a variable intensity fiber optic light source (Fiber-Lit-PL800, Dolan-Jenner Industries, Boxborough, MA, USA) was taken to determine the outline of each slice. Fluorescence images were later superimposed on the white light images for visualization of the reference and array shank points. The brain was then reconstructed in three dimensions using Rhinoceros (Seattle, WA, USA), and the positions of the arrays were estimated by creating best fit lines through the points on individual slices.

Reconstructions for each brain were normalized to one standard brain, guided by the curvature of the IC and a reference needle point at the intersection of the superior colliculus, thalamus, and lateral extension from the IC. This reference point is consistent across animals and serves as a critical landmark for normalizing and aligning the different brains with each other (for further details and images, see (Markovitz et al., 2012)). Isofrequency laminae were approximated by creating a plane orthogonal to the average insertion angle of all best fit lines of each array placement. The depth of each lamina was determined by calculating the distance from the surface of the IC, where neurons do not respond to broadband noise, to locations where neurons respond with specific BFs (Markovitz et al., 2012). This distance was

multiplied by a scaling factor to account for tissue changes due to the histological process.

A total of 437 ICC sites were stimulated. Given that some ICC sites were paired with both AI and VRB sites, 141 ICC sites were paired with at least one AI site and 312 ICC sites were paired with at least one VRB site. To analyze location effects across the ICC lamina, we created four laminae that would include the majority of sites at the following frequencies: 1.1–1.7 kHz (N = 51 ICC sites), 3.8–6.1 kHz (N = 44), 6.2–10 kHz (N = 107) and 11–17 kHz (N = 72).We chose each lamina to have a bandwidth of approximately 0.6 octaves, which corresponds to two critical bands (Schreiner and Langner, 1997; Malmierca et al., 2008), in order to have sufficient points for analysis. If there was more than one ICC site for a placement within the frequency lamina, the site resulting in the lowest threshold antidromic activity was chosen for data analysis. Locations of all array positions on the normalized brain can be seen in Fig. 4A along with the four isofrequency laminae. ICC locations within each laminae were determined and represented as circles or triangles dependent on the recording sub-region in AC in Fig. 4B.

RESULTS

Overview of approach

We compared corticofugal projections to the ICC arising from AI and VRB (Fig. 1) to determine if these tonotopically organized cortical areas have different projection patterns across the ICC. Corticofugal projections were identified when layer V sites in the AC had antidromic activity in response to electrical stimulation of the ICC with the specific characteristics described in *Experimental procedures*. In the following sections, we characterize these corticocollicular projections by analyzing their tonotopic arrangement and spatial distribution across the AC as well as across the isofrequency laminae of the ICC.

Tonotopic arrangement of descending projections

The first goal of this project was to confirm tonotopically organized corticofugal projections from AI to ICC found previously and to assess the corticofugal organization from VRB. We initially determined how the frequency specificity of the fibers related to the current level was used for stimulation. For each ICC–AC stimulation-recording site pair where antidromic activity was detected, we determined the threshold of stimulation that elicited antidromic activity and compared it to the difference in BF (**ΔBF**) between the two sites. We found that as the stimulation threshold increased, the ΔBF between AI and ICC also increased (Fig. 5A). A similar trend for VRB and ICC can be seen in Fig. 5B, though the BF mismatch was much larger with the VRB sites in comparison to the AI sites, even at thresholds below 30 μA. Using a two-way ANOVA to fit ΔBF with a linear model on the factors of threshold and AC placement (i.e., VRB or A1), we found that both threshold ($P < 0.002$) and AC placement ($P < 4 \times 10^{-15}$) were significant factors (N = 154 AI points, N = 134 VRB points). Therefore, greater ΔBFs are often found at high thresholds and when recording antidromic activity in VRB.

Considering that high stimulation levels could be activating fibers from other laminae because of greater current spread and neural activation, we only investigated activity evoked by lower stimulation levels in the second part of this analysis. The stimulation level criterion was determined from our data as well as data from Lim and Anderson (2007a), both demonstrating that most AI–ICC antidromic thresholds occurred below 32 μA, which corresponds to a maximal spread of

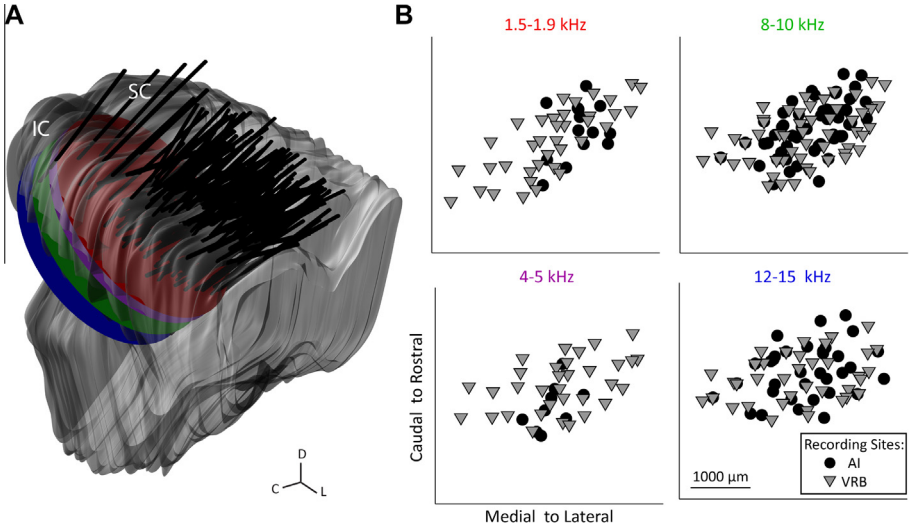

Fig. 4. Histological reconstructions and placements of each stimulation location within the ICC and across isofrequency laminae of the ICC. (A) The midbrains and array placements were reconstructed in three dimensions and normalized onto a single brain. Each placement was determined to be in the ICC due to the presence of tonotopic shifts of increasing BFs with deeper sites for each shank (see *Methods: placement of arrays*). The four isofrequency laminae (circular planes) were approximated as a plane at a depth where neurons respond at those BFs. (B) Each ICC site was electrically stimulated and activity was elicited in either VRB (triangles) or AI (circles). C, caudal; D, dorsal; SC, superior colliculus.

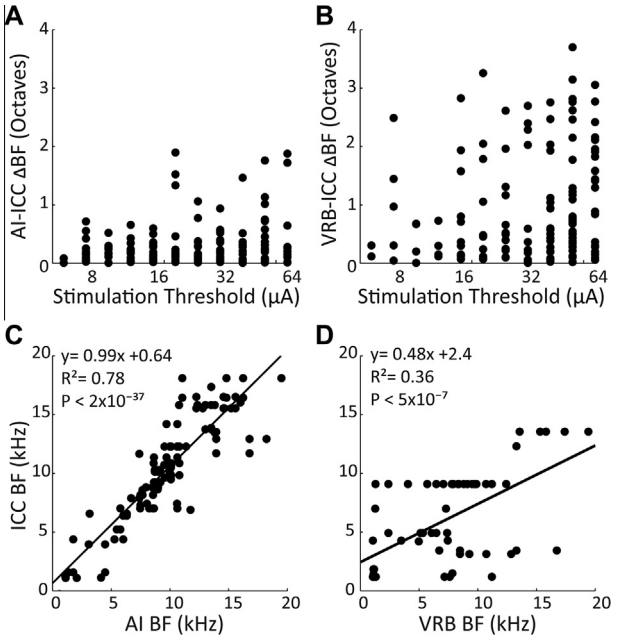

Fig. 5. ICC sites that evoke antidromic activity in the cortex have BFs that are more similar to sites in AI than sites in VRB, especially at low stimulation levels. For each AC–ICC site pair with a monosynaptic projection, the ΔBF between each site pair was correlated to the minimum amount of current necessary to evoke antidromic activity. For both AI (A) and VRB (B), the higher stimulation thresholds activate sites that have greater BF-mismatch, though neurons in AI show more similar BFs to the ICC than do neurons in VRB. For corticofugal projections where antidromic activity was observed in the AC at low stimulation levels (⩽32 μA), the BF of the stimulation site in ICC was correlated to the recording site in AI (C) or VRB (D). While a strict tonotopy was found for corticofugal projections from AI, weak tonotopy was observed for projections from VRB.

approximately 250 μm (Ranck, 1975; Lim and Anderson, 2007a). Using this level provided sufficient spatial discrimination while limiting maximum current spread in our analysis. Since each frequency lamina is approximately 175 μm in cat (Schreiner and Langner, 1997) and 150 μm in rat (Malmierca et al., 2008), which should be similar to the lamina in guinea pig, a current level of 32 μA would activate one or two laminae. We decided (demonstrated later in Fig. 5C) that this extent of spatial discrimination along the tonotopic axis would be sufficient for the objective of this study while still allowing enough points for analysis: for site pairs with antidromic activity, 71% (110 out of 154 sites) of AI–ICC pairs and 45% (60 out of 134 sites) of VRB–ICC pairs occurred at stimulation levels at or below 32 μA.

Next, we wanted to assess tonotopicity of corticofugal projections at low stimulation thresholds, first for AI and second for VRB. For cases where antidromic activity was elicited at thresholds equal to or below 32 μA, Fig. 5C shows that the BF of the AI recording site was similar to the BF of the stimulating ICC site, with the average ΔBF of 0.2 ± 0.3 octaves for AI–ICC sites (N = 110 pairs). Since linear regression found a significant correlation between the BFs ($P < 2 \times 10^{-37}$), we conclude that corticofugal projections from AI are tonotopically organized. As mentioned above, even if levels up to 32 μA cause some current spread of activation, Fig. 5C demonstrates that the extent of spread was not large enough to mask our ability to detect the tonotopic pattern. Fig. 5D shows that the BFs of VRB and ICC sites were also significantly correlated ($P < 5 \times 10^{-7}$), though the mismatch between the two sites was greater at 0.8 ± 0.9 octaves for VRB–ICC sites (N = 60 pairs). This mismatch cannot be solely due to current spreading onto other isofrequency laminae in the ICC as confirmed by the AI results. Instead, this mismatch is indicative of an anatomical organization where a given isofrequency lamina in the ICC contains antidromic projections from VRB areas with more variance in BFs than that observed from AI.

Location effects of corticofugal projections

We first investigated whether any spatial distribution of the corticofugal projections exists across AI and VRB. We did not observe any clear spatial trends in organization; antidromic activity fully spanned across AI and VRB, as outlined in Fig. 1. We also determined the minimum stimulation threshold across all relevant ICC sites that evoked antidromic activity at each cortical location, and found no correlation between the recording location in AI or VRB and the minimum threshold value. While we did not find location differences across the cortex, we did find differences in the prevalence of projections to AI versus VRB. Electrical stimulation of 60% (84 out of 141 sites) of ICC sites caused antidromic activity of at least one site in AI at or below our maximum stimulation level (64 μA). In contrast, 31% (98 out of 312 sites) of ICC sites antidromically activated at least one VRB site. In addition, we found FSL of antidromic activity for fibers originating in AI and VRB (Fig. 6). The mean FSL for VRB projections was 8.1 ± 3.5 ms (N = 134 sites), which was significantly longer than the mean FSL of AI, 6.5 ± 2.3 ms (N = 154 sites; $P < 5.8 \times 10^{-5}$ using the Mann–Whitney U test). Notably, the long-latency example shown in Fig. 3 was recorded in the VRB. The longer latency of VRB projections is likely due to these axons being thinner, having slower conduction, and/or traversing a longer route than AI projections. Therefore, fibers from AI are more prevalent and faster in latency than fibers from VRB.

Secondly, we examined location trends across the isofrequency laminae of the ICC. ICC stimulation sites were separated into four isofrequency laminae based on their BF, and the minimum stimulation threshold for each ICC site that evoked antidromic activity on any relevant AC site was determined. The location of each ICC stimulation site was determined within the respective lamina using histological reconstructions of each array placement and midbrain (see *Experimental procedures: Histological reconstructions*). ICC sites with BFs beyond the bandwidth for each lamina were excluded from this analysis. For each ICC site, the lowest threshold that evoked antidromic activity either in AI or VRB was determined. Since we established that these descending projections were primarily tonotopically organized, we compared AC sites that were BF-matched to each ICC site. Sites were

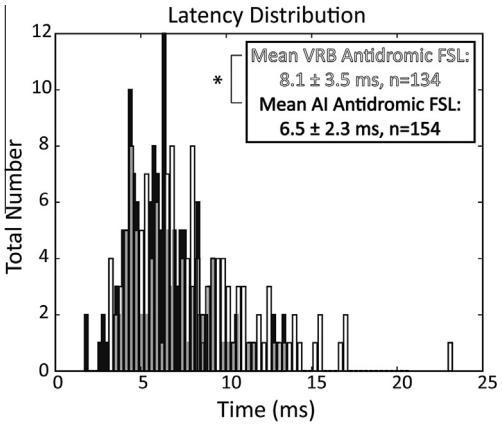

Fig. 6. The FSLs for antidromic activity evoked in AI was significantly shorter than antidromic activity evoked in VRB ($P < 5.8 \times 10^{-5}$ using the Mann–Whitney *U* test).

determined to be BF-matched when ΔBF's were less than 0.3 octaves (the standard deviation of the AI–ICC ΔBFs at thresholds below 32 μA).

As shown in Fig. 7A, there was no obvious trend for minimal AI stimulation threshold across any of the four isofrequency laminae. Although the lower frequency laminae had fewer points that did not fully span the extent of the lamina, these data support the well-sampled data at the higher frequency laminae, which found that stimulation of a wide span of locations throughout the ICC could result in cortical antidromic activation.

While AI tonotopic corticofugal fibers were present throughout the ICC lamina, VRB corticofugal fibers that were BF-matched could be activated more frequently in the caudal–medial region of all four laminae, as shown in Fig. 7B. Each lamina was separated into a caudal–medial and a rostral–lateral half as indicated by the line in each pane, using the average location of all points as the center of a line with a 45° angle (where 0° would be the caudal to rostral axis and 90° would be the medial to lateral axis). The percentage of sites within each half that elicited antidromic activation in VRB was greater in the caudal–medial half of each lamina, as indicated in each pane in Fig. 7B. Across all laminae, corticofugal projections were evident when stimulating 8% of the sites in rostral–lateral regions as compared to 28% of the sites in the caudal–medial regions.

Given that VRB corticofugal fibers in general had greater mismatch in BF than AI fibers, we further expanded the ICC location analysis for VRB corticofugal fibers to include BF-unmatched sites. We plotted the location of ICC sites with their minimum stimulation threshold across all VRB sites, regardless of BF, in Fig. 7C. In comparison to the BF-matched-only connections in Fig. 7B, a greater percentage of sites throughout each laminae had corticofugal projections to at least one VRB site with any BF value. However, the rostral–lateral regions still had a smaller percentage of sites with corticofugal projections, with a total of 19% versus 47% of sites responding in the rostral–lateral versus caudal–medial regions, respectively. To further test for significance in antidromic threshold differences in VRB for the rostral–lateral versus caudal–medial ICC regions, we also combined all of the ICC laminae together and compared thresholds between these two regions. Since thresholds were collected in 2 dB increments, we compared these thresholds on a dB scale, and for locations where thresholds could not be detected, we set the max threshold at 80 μA (i.e., 2 dB above our max stimulation level [see *Experimental procedures*: *Electrical stimulation and data analysis*]). We found the thresholds in the rostral–lateral region were significantly higher than those in the caudal–medial region ($P < 3 \times 10^{-5}$ using the Mann–Whitney *U* test). Therefore, for antidromically activated projections from VRB that are both well- and poorly-matched in BF to ICC neurons, they are more frequently found in caudal–medial rather than rostral–lateral areas of the isofrequency laminae in the ICC. The sparsity of VRB projections in the rostral–lateral region could have resulted in the higher thresholds observed in that region, requiring a greater current spread on average to activate the nearest axon for a given ICC site.

DISCUSSION

Our results demonstrate that corticofugal fibers from AI have a strict tonotopic organization that is distributed throughout an isofrequency lamina of the ICC, confirming a previous study (Lim and Anderson, 2007a). In contrast to AI, fibers from VRB to ICC exhibit greater mismatch in tonotopic organization and more heavily project to the caudal–medial region within the ICC laminae. Additionally, there are also fewer projections from VRB than from AI to the ICC. The differences in corticofugal projections from AI and VRB in relation to spatial distribution and frequency organization suggest these two cortical areas have different roles within the descending auditory system.

Methodological considerations of antidromic stimulation

Using antidromic stimulation as a method to study the spatial distribution of monosynaptic corticofugal projections allowed us to characterize the anatomical and physiological properties of neurons with greater spatial resolution in the cortex and ICC compared to traditional tracer techniques. Specifically, tracer injections into the small region of VRB would likely diffuse into the lateral area of AI, and thus differentiation between the two regions would be more difficult.

Though the antidromic stimulation method has many benefits, caution must be used in the interpretation of our results because of some important limitations. One drawback is that stimulation of ICC regions may have caused antidromic activity in cortical regions that were not sampled since we could simultaneously record from only four AI locations at a time with our specific electrode array. This undersampling could have limited the ability to observe spatial patterns across AI or VRB, potentially obscuring more complex topographic patterns of the corticofugal projections. Note that customized and

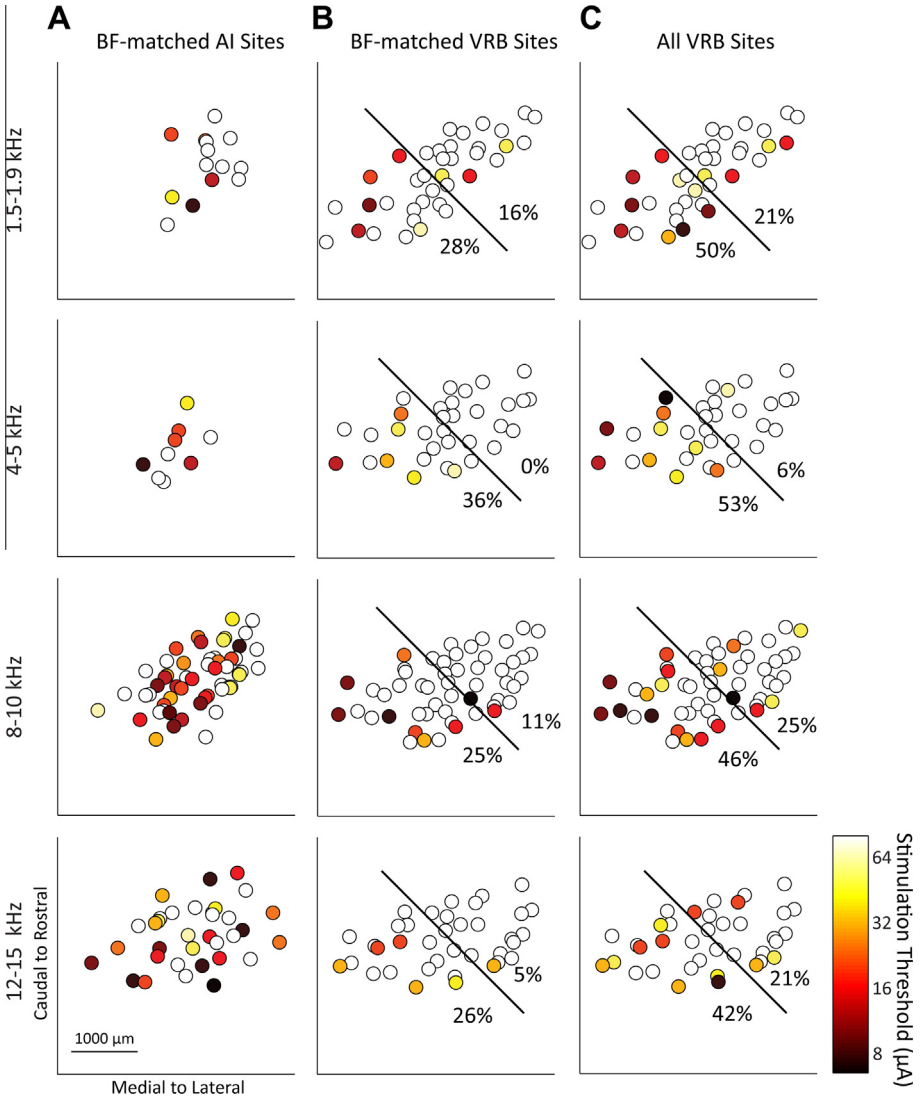

Fig. 7. Comparing the locations of sites across ICC laminae shows differential maps of minimal thresholds for antidromic activity found in BF-matched sites in AI, BF-matched sites in VRB, and all sites in VRB. At each location across the four ICC isofrequency laminae, the minimum stimulation thresholds evoked from BF-matched AI sites (A), BF-matched VRB sites (B), or all VRB sites (C) were found. ICC sites that could not elicit antidromic activity in any cortical site even at the highest stimulation threshold (64 μA) are marked as white. While no spatial trend was observed across the ICC lamina for AI corticofugal projections, VRB fibers were typically found in more caudal–medial regions of the ICC. For VRB projections (B and C), each lamina was split into a caudal–medial and rostral–lateral half (based on the average location of all measured sites), and the percentage of sites that evoked antidromic activity was found for each half.

higher density electrode arrays can be used in future studies to achieve a greater sampling of neurons and locations in each animal. The second drawback is that antidromic stimulation could have activated axon terminals as well as passing fibers. Stimulation of a given ICC location may have caused antidromic activity in the cortex from corticofugal fibers directly innervating that region or passing through that location en route to other neurons. Therefore, we can conclude that AI corticofugal fibers pass and/or terminate throughout an ICC lamina in a strictly tonotopic organization, while VRB corticofugal fibers pass and/or terminate within more caudal–medial locations of an ICC lamina in an approximately tonotopic pattern. Despite this limitation, it is unlikely that these projections would exclusively traverse across an entire ICC lamina without synapsing onto any neurons, especially while maintaining a precise tonotopic organization from AC, if there was not a functional role for these projections within the ICC.

Tonotopic organization of corticocollicular projections

These results confirm that AI corticofugal projections generally exhibit a tonotopic organization. Of the projections that could be activated with relatively low current levels ($\leqslant$32 μA), the average ΔBF was 0.2 ± 0.3 octaves, similar to the bandwidth of an ICC isofrequency lamina (Schreiner and Langner, 1997; Malmierca et al., 2008). This suggests that frequency-specific AI corticofugal fibers generally remain within an isofrequency lamina of the ICC. Projections originating

in VRB are loosely tonotopically organized, with an average ΔBF of 0.8 ± 0.9 octaves for fibers with thresholds equal to or below 32 μA. The weaker tonotopic organization shown in Fig. 5 for VRB in comparison to AI could be associated with a more diffused projection pattern to the ICC and/or a weaker tonotopic organization directly within VRB (Wallace et al., 2000).

Isofrequency organization of corticocollicular projections

Our results provide evidence that corticofugal projections from AI and VRB are present in the ICC. For corticofugal fibers originating from both AI and VRB, antidromic activation could be elicited even with low stimulation thresholds of less than 12 μA, which corresponds to a maximal current spread distance of ~150 μm (i.e., a distance smaller than the diameter of the circular symbols in Fig. 4) (Ranck, 1975; Lim and Anderson, 2007a). With such low stimulation thresholds at central regions of the lamina, it would be unlikely that current could spread beyond the borders of the ICC and activate the corticofugal projections in the cortices of the IC. Thus, we conclude that corticofugal projections from both AI and VRB exist within the ICC, with fibers originating from AI being distributed throughout an ICC lamina and fibers originating from VRB more frequently targeting the caudal–medial versus rostral–lateral regions of an ICC lamina.

Lack of spatial organization of AI corticofugal projections along an ICC lamina was unexpected considering that activation of AI resulted in excitatory responses mainly in caudal–medial and not rostral–lateral regions of an ICC lamina in a previous study (Markovitz et al., 2013). This difference between the anatomical projections found here and previous physiological functional projections could be due to existence of many polysynaptic projections from AI to the ICC: activating AI neurons could have resulted in the excitation of neurons either in other cortical areas or in the cortices of the IC. These regions could then excite the ICC mainly in the caudal–medial regions while restricting activity in the rostral–lateral regions. An alternative possibility in this study is that the corticofugal projections from AI could be passing through rostral–lateral regions of the ICC en route to their target of the caudal–medial regions, and electrical stimulation of the ICC with our antidromic method activated these passing fibers. However, this would not explain why more antidromic cases were not observed in the rostral–lateral region of the ICC for VRB, unless there is a different trajectory for VRB projections to reach the caudal–medial region of the ICC. It is also possible that the corticofugal neurons from AI terminate throughout the ICC but that inhibition plays a more dominant role in the rostral–lateral portion that somehow restricts excitatory responses.

Comparisons to other species

There have been mixed results across multiple studies relating to the presence and organization of corticofugal fibers targeting the ICC from AI. Several studies found that corticofugal projections primarily or exclusively target the external cortices of the IC (Faye-Lund, 1985; Huffman and Henson, 1990; Herbert et al., 1991; Winer et al., 1998). While it is clear that the presence of corticocollicular projections are more dense in the external cortices, several other studies using larger injection volumes of stable tracers have found evidence of tonotopic projections to the ICC in cat, ferret, rat, guinea pig and gerbil (Andersen et al., 1980; Feliciano and Potashner, 1995; Saldana et al., 1996; Budinger et al., 2000; Bajo and Moore, 2005; Coomes et al., 2005; Bajo et al., 2007; Lim and Anderson, 2007a; Malmierca and Ryugo, 2011). Our results provide further evidence that these projections are present in the ICC and are strictly tonotopic in nature. We also found AI projections to be amply scattered throughout an isofrequency lamina, similar to a previous antidromic stimulation study (Lim and Anderson, 2007a).

In addition to the corticofugal projections from AI, we discovered that VRB has monosynaptic corticofugal projections to the ICC, which confirms a previous study in guinea pig that used a retrograde tracer injection into the IC and detected corticofugal projections from layer V cells of the AC, including cortical regions that correspond to VRB (Schofield, 2009). Due to similarities in long response latencies to pure tones and tonotopic organization, VRB is likely related to the ventral auditory field (**VAF**) in rat (Polley et al., 2007; Storace et al., 2010) and either the dorsoposterior or ventroposterior field in gerbil (Thomas et al., 1993). VAF is thought to be a ventral margin of Te1 (Polley et al., 2007), which has corticocollicular projections targeting the ICC (Saldana et al., 1996). In gerbil, Budinger et al. (2000) found that corticocollicular projections from the dorsoposterior and ventroposterior fields appear similar and have moderate projections targeting the ipsilateral ICC, though a more recent study found that corticocollicular projections from these fields only target the external cortices and exclude the ICC (Bajo and Moore, 2005). Within cats and ferrets, projections to the ICC were found from primary regions, but not non-primary or non-core regions that would include areas most similar to VRB (Winer et al., 1998; Winer, 2005; Bajo et al., 2007). Overall, it is still unclear whether regions similar to VRB across species have corticofugal projections to the ICC. It may be that tracer studies were unable to detect corticofugal projections from VRB-like regions for three main reasons. First, some corticocollicular mapping studies that did not observe projections could have had tracers that were not sufficiently detecting the thin VRB fibers. Projections from VRB may have fibers that are even thinner than those from A1, which is supported by the longer latencies of antidromic activity in VRB versus AI (Fig. 6). Second, these projections are even less prevalent than those from AI, and thus potentially more difficult to detect. Third, these projections are most often observed in caudal–medial regions of the ICC (Fig. 7), and differences in cytoarchitectonic criteria may have resulted in different boundaries of the ICC across studies.

Conclusions and future directions

In this study, we found that, like AI, VRB has descending corticofugal projections to the ICC that are organized tonotopically, though those from VRB are fewer, have a weaker tonotopic organization, and are found mostly in the caudal–medial regions of the ICC. The role of these corticofugal projections is still not understood. Corticocollicular projections originating from AI are thought to modulate ascending auditory activity and mediate plastic changes (Yan and Suga, 1998; Yan et al., 2005; Xiong et al., 2009). Given that VRB is thought to be important for speech understanding (Grimsley et al., 2012), the projections from VRB to ICC could provide one way in which the brain can directly modulate and enhance coding to natural stimuli through the ascending lemniscal pathway. Having shown that anatomical and physiological differences exist between corticocollicular fibers from AI and VRB in this study, future studies should investigate the anatomical organization and functional role of corticofugal fibers from VRB and other cortical regions beyond AI that project to different subcortical targets. These studies will further our understanding of how the auditory brain modulates ascending sound information. These studies also have clinical implications for treating hearing disorders such as tinnitus. To date, over 50 patients have been implanted with electrode arrays that electrically stimulate secondary cortical regions to treat tinnitus (Friedland et al., 2007; De Ridder et al., 2011; Vanneste and De Ridder, 2012; Zhang, 2013; Engelhardt et al., 2014). A greater understanding of the functional organization of descending and modulatory projections from these secondary or non-core cortical regions to the auditory system could help identify more appropriate neural targets and more effective stimulation strategies for treating tinnitus.

CONFLICTS OF INTEREST

None.

Acknowledgements—The authors would like to thank Sarah Offutt for her thoughtful criticism of this work. This work was supported by start-up funds from the University of Minnesota – United States and NIH NIDCD – United States R03DC011589.

REFERENCES

Abeles M, Goldstein Jr MH (1970) Functional architecture in cat primary auditory cortex: columnar organization and organization according to depth. J Neurophysiol 33:172–187.

Andersen RA, Snyder RL, Merzenich MM (1980) The topographic organization of corticocollicular projections from physiologically identified loci in the AI, AII, and anterior auditory cortical fields of the cat. J Comp Neurol 191:479–494.

Anderson DJ, Najafi K, Tanghe SJ, Evans DA, Levy KL, Hetke JF, Xue XL, Zappia JJ, Wise KD (1989) Batch-fabricated thin-film electrodes for stimulation of the central auditory system. IEEE Trans Biomed Eng 36:693–704.

Bajo VM, Moore DR (2005) Descending projections from the auditory cortex to the inferior colliculus in the gerbil, Meriones unguiculatus. J Comp Neurol 486:101–116.

Bajo VM, Nodal FR, Bizley JK, Moore DR, King AJ (2007) The ferret auditory cortex: descending projections to the inferior colliculus. Cereb Cortex 17:475–491.

Budinger E, Heil P, Scheich H (2000) Functional organization of auditory cortex in the Mongolian gerbil (*Meriones unguiculatus*). IV. Connections with anatomically characterized subcortical structures. Eur J Neurosci 12:2452–2474.

Coomes DL, Schofield RM, Schofield BR (2005) Unilateral and bilateral projections from cortical cells to the inferior colliculus in guinea pigs. Brain Res 1042:62–72.

De Ridder D, Vanneste S, Kovacs S, Sunaert S, Menovsky T, van de Heyning P, Moller A (2011) Transcranial magnetic stimulation and extradural electrodes implanted on secondary auditory cortex for tinnitus suppression. J Neurosurg 114(4):903–911.

Eggermont JJ, Roberts LE (2004) The neuroscience of tinnitus. Trends Neurosci 27(11):676–682.

Engelhardt J, Dauman R, Arne P, Allard M, Dauman N, Branchard O, Perez P, Germain C, Caire F, Bonnard D, Cuny E (2014) Effect of chronic cortical stimulation on chronic severe tinnitus: a prospective randomized double-blind cross-over trial and long-term follow up. Brain Stimul 7(5):694–700.

Faye-Lund H (1985) The neocortical projection to the inferior colliculus in the albino rat. Anat Embryol (Berl) 173:53–70.

Feliciano M, Potashner SJ (1995) Evidence for a glutamatergic pathway from the guinea pig auditory cortex to the inferior colliculus. J Neurochem 65:1348–1357.

Ferster D, Lindstrom S (1983) An intracellular analysis of geniculo-cortical connectivity in area 17 of the cat. J Physiol 342:181–215.

Friedland DR, Gaggl W, Runge-Samuelson C, Ulmer JL, Kopell BH (2007) Feasibility of auditory cortical stimulation for the treatment of tinnitus. Otol Neurotol 28(8):1005–1012.

Grimsley JM, Shanbhag SJ, Palmer AR, Wallace MN (2012) Processing of communication calls in Guinea pig auditory cortex. PLoS One 7:e51646.

Herbert H, Aschoff A, Ostwald J (1991) Topography of projections from the auditory cortex to the inferior colliculus in the rat. J Comp Neurol 304:103–122.

Huang CL, Winer JA (2000) Auditory thalamocortical projections in the cat: laminar and areal patterns of input. J Comp Neurol 427:302–331.

Huffman RF, Henson Jr OW (1990) The descending auditory pathway and acousticomotor systems: connections with the inferior colliculus. Brain Res Brain Res Rev 15:295–323.

Kral A, Hartmann R, Tillein J, Heid S, Klinke R (2000) Congenital auditory deprivation reduces synaptic activity within the auditory cortex in a layer-specific manner. Cereb Cortex 10:714–726.

Lenarz M, Lim HH, Patrick JF, Anderson DJ, Lenarz T (2006) Electrophysiological validation of a human prototype auditory midbrain implant in a guinea pig model. J Assoc Res Otolaryngol 7:383–398.

Lim HH, Anderson DJ (2006) Auditory cortical responses to electrical stimulation of the inferior colliculus: implications for an auditory midbrain implant. J Neurophysiol 96:975–988.

Lim HH, Anderson DJ (2007a) Antidromic activation reveals tonotopically organized projections from primary auditory cortex to the central nucleus of the inferior colliculus in guinea pig. J Neurophysiol 97:1413–1427.

Lim HH, Anderson DJ (2007b) Spatially distinct functional output regions within the central nucleus of the inferior colliculus: Implications for an auditory midbrain implant. J Neurosci 27:8733–8743.

Lipski J (1981) Antidromic activation of neurons as an analytic tool in the study of the central nervous system. J Neurosci Methods 4:1–32.

Malmierca M, Ryugo D (2011) Descending Connections of Auditory Cortex to the Midbrain and Brain Stem. In: Winer JA, Schreiner CE, editors. The Auditory Cortex. US: Springer. p. 189–208.

Malmierca MS, Rees A, Le Beau FE, Bjaalie JG (1995) Laminar organization of frequency-defined local axons within and between the inferior colliculi of the guinea pig. J Comp Neurol 357:124–144.

Malmierca MS, Izquierdo MA, Cristaudo S, Hernandez O, Perez-Gonzalez D, Covey E, Oliver DL (2008) A discontinuous tonotopic

organization in the inferior colliculus of the rat. J Neurosci 28:4767–4776.
Markovitz CD, Tang TT, Edge DP, Lim HH (2012) Three-dimensional brain reconstruction of *in vivo* electrode tracks for neuroscience and neural prosthetic applications. Front Neural Circuit 6.
Markovitz CD, Tang TT, Lim HH (2013) Tonotopic and localized pathways from primary auditory cortex to the central nucleus of the inferior colliculus. Front Neural Circuits 7:77.
Middlebrooks JC (2008) Auditory cortex phase locking to amplitude-modulated cochlear implant pulse trains. J Neurophysiol 100:76–91.
Mitani A, Shimokouchi M (1985) Neuronal connections in the primary auditory cortex: an electrophysiological study in the cat. J Comp Neurol 235:417–429.
Mitzdorf U (1985) Current source-density method and application in cat cerebral cortex: investigation of evoked potentials and EEG phenomena. Physiol Rev 65:37–100.
Muller-Preuss P, Mitzdorf U (1984) Functional anatomy of the inferior colliculus and the auditory cortex: current source density analyses of click-evoked potentials. Hear Res 16:133–142.
Neuheiser A, Lenarz M, Reuter G, Calixto R, Nolte I, Lenarz T, Lim HH (2010) Effects of pulse phase duration and location of stimulation within the inferior colliculus on auditory cortical evoked potentials in a guinea pig model. J Assoc Res Otolaryngol 11:689–708.
Polley DB, Read HL, Storace DA, Merzenich MM (2007) Multiparametric auditory receptive field organization across five cortical fields in the albino rat. J Neurophysiol 97:3621–3638.
Ranck Jr JB (1975) Which elements are excited in electrical stimulation of mammalian central nervous system: a review. Brain Res 98:417–440.
Redies H, Brandner S, Creutzfeldt OD (1989a) Anatomy of the auditory thalamocortical system of the guinea pig. J Comp Neurol 282:489–511.
Redies H, Sieben U, Creutzfeldt OD (1989b) Functional subdivisions in the auditory cortex of the guinea pig. J Comp Neurol 282:473–488.
Rose HJ, Metherate R (2001) Thalamic stimulation largely elicits orthodromic, rather than antidromic, cortical activation in an auditory thalamocortical slice. Neuroscience 106:331–340.
Saldana E, Feliciano M, Mugnaini E (1996) Distribution of descending projections from primary auditory neocortex to inferior colliculus mimics the topography of intracollicular projections. J Comp Neurol 371:15–40.
Schofield BR (2009) Projections to the inferior colliculus from layer VI cells of auditory cortex. Neuroscience 159:246–258.
Schofield BR, Coomes DL (2006) Pathways from auditory cortex to the cochlear nucleus in guinea pigs. Hear Res 216–217:81–89.
Schofield BR, Hallman LE, Lin CS (1987) Morphology of corticotectal cells in the primary visual cortex of hooded rats. J Comp Neurol 261(1):85–97.
Schreiner CE, Langner G (1997) Laminar fine structure of frequency organization in auditory midbrain. Nature 388:383–386.
Schreiner CE, Read HL, Sutter ML (2000) Modular organization of frequency integration in primary auditory cortex. Annu Rev Neurosci 23:501–529.
Smith PH, Populin LC (2001) Fundamental differences between the thalamocortical recipient layers of the cat auditory and visual cortices. J Comp Neurol 436:508–519.
Snyder RL, Bierer JA, Middlebrooks JC (2004) Topographic spread of inferior colliculus activation in response to acoustic and intracochlear electric stimulation. J Assoc Res Otolaryngol 5:305–322.
Storace DA, Higgins NC, Read HL (2010) Thalamic label patterns suggest primary and ventral auditory fields are distinct core regions. J Comp Neurol 518:1630–1646.
Straka MM, Schendel D, Lim HH (2013) Neural integration and enhancement from the inferior colliculus up to different layers of auditory cortex. J Neurophysiol 110:1009–1020.
Swadlow HA (1998) Neocortical efferent neurons with very slowly conducting axons: strategies for reliable antidromic identification. J Neurosci Methods 79(2):131–141.
Thomas H, Tillein J, Heil P, Scheich H (1993) Functional organization of auditory cortex in the mongolian gerbil (Meriones unguiculatus). I. Electrophysiological mapping of frequency representation and distinction of fields. Eur J Neurosci 5:882–897.
Vanneste S, De Ridder D (2012) Noninvasive and invasive neuromodulation for the treatment of tinnitus: an overview. Neuromodulation 15(4):350–360.
Wallace MN, Palmer AR (2008) Laminar differences in the response properties of cells in the primary auditory cortex. Exp Brain Res 184:179–191.
Wallace MN, Rutkowski RG, Palmer AR (1999) A ventrorostral belt is adjacent to the guinea pig primary auditory cortex. Neuroreport 10:2095–2099.
Wallace MN, Rutkowski RG, Palmer AR (2000) Identification and localisation of auditory areas in guinea pig cortex. Exp Brain Res 132:445–456.
Winer JA (2005) Decoding the auditory corticofugal systems. Hear Res 207:1–9.
Winer JA, Larue DT, Diehl JJ, Hefti BJ (1998) Auditory cortical projections to the cat inferior colliculus. J Comp Neurol 400:147–174.
Xiong Y, Zhang Y, Yan J (2009) The neurobiology of sound-specific auditory plasticity: a core neural circuit. Neurosci Biobehav Rev 33:1178–1184.
Yan W, Suga N (1998) Corticofugal modulation of the midbrain frequency map in the bat auditory system. Nat Neurosci 1:54–58.
Yan J, Zhang Y, Ehret G (2005) Corticofugal shaping of frequency tuning curves in the central nucleus of the inferior colliculus of mice. J Neurophysiol 93:71–83.
Zhang J (2013) Auditory cortex stimulation to suppress tinnitus: mechanisms and strategies. Hear Res 295:38–57.

(Accepted 14 May 2015)
(Available online 19 May 2015)